Food procurement of staple cereals for world major cities in 2050

Toshichika Iizumi [1, *], Takahiro Takimoto [1], Michiya Hayashi [2], Hideo Shiogama [2], Shinichiro Fujimori [3], Tomoko Hasegawa [4]

[1] National Agriculture and Food Research Organization, Tsukuba, Japan
[2] National Institute for Environmental Studies, Tsukuba, Japan
[3] Graduate School of Engineering, Kyoto University, Kyoto, Japan
[4] Research Organization of Science and Technology, Ritsumeikan University, Kusatsu, Japan

Correspondence: Toshichika Iizumi (iizumit@affrc.go.jp)

Abstract

Cities are dependent on food transported domestically or internationally. However, little is known about how the burden of transporting food to cities will changes under future socio-economic and climatic conditions. Here we present the current transport loads of major commodities (wheat and rice) and their projections in 2050 for 208 world's major cities, using food-miles as a metric. The estimated freight transport routes and resulting distance-sufficiency curves characterized the cities well and provided insights to improve the robustness of food procurement. The least food-miles required to achieve 70% of the city's wheat (rice) demand in 2050 were projected to increase in 68 (85) cities and decrease in 61 (54) cities, compared to the variations in food-miles associated with the current natural climate variability, with 79 (54) cities remaining unchanged. These findings provide city-specific information that ultimately helps to plan for more robust food procurement in the context of climate-resilient cities.

Cities are hubs of economic activity and residence for 55% of the world's 8 billion people in 2018 (United Nations 2019). The rapid shift to urban living is increasing the reliance on transported food, both domestically and internationally (Seto and Ramankutty 2016). Food supply chains are fundamental to supporting urban living and are highly dependent on infrastructure and services, such as freight transport, storage, wholesale and retail. This fact has been repeatedly demonstrated over the last decade by the supply disruptions caused by the food crises (Ruel et al. 2010, Miller et al. 2024), pandemics (Gomez et al. 2021) and wars (Nóia Júnior et al. 2022).

Accumulated evidence indicates that projected warming and changes in precipitation patterns would disproportionately affect the productivity of staple cereals between the low and high latitudes (Jägermeyr et al. 2021). Other projected changes also include the exacerbation of production stability and the risk of multi-breadbasket crop failures (Hasegawa et al. 2022, Chen et al. 2024), poleward shift of areas suitable for cropping (Zabel et al. 2024), and food price increases affecting vulnerable groups of urban residents in import-dependent countries (Zhang et al. 2022). The growing urban population, which is expected to reach 68% of 9.8 billion in 2050 (United Nations 2019), will occur alongside these changes in food availability and access. Food access in cities may be further compromised by rural out-migration to urban settlements, internally or abroad (Tuholske et al. 2024). Therefore, transforming urban agri-food systems, including food procurement, to be more robust to these changes is important as part of the climate-resilient development (Dodman et al. 2022).

However, while the projected climate impacts mentioned above are relevant at the national to sub-national levels, it is difficult to derive direct implications for individual cities. The lack of city-specific information prevents urban planners and managers of infrastructure and services from taking countermeasures to make food procurement more robust to the changes. To fill this gap, this study aims to present the projected changes in transport loads of the major commodities, wheat and rice, for 208 major cities around the world in 2050 under the future scenarios of demographics, crop area and climate impacts on crop yields. Food-miles is chosen as the main metric to quantify transport loads. Food consumed in cities is transported by freight transport from production areas, domestically or internationally. Increasing dependence on food imports is a common trend in many countries and probably many cities (d'Amour and Weston 2020). Projections of freight transport loads is therefore vital as a first step to prepare for the expected socio-economic and climatic conditions in the coming decades. For this, we combinedly used the Dijkstra algorithm with the road and vessel density map to estimate plausible global freight transport routes and resulting food-miles for each city.

Wheat and rice are selected for this study because of their importance in human food consumption and for their contrasting characteristics in international trade. Together, these crops provide nearly 40% of calories and 30% of protein for humans on a global average (Xia et al. 2022). Wheat is a daily staple for 2.5 billion people worldwide (CIMMYT 2019), while rice is eaten by 4 billion people in the most populated regions, Asia and Africa (IRRI 2023). Focusing on the countries trading over 1,000 tons in 2022, 64 countries exported 1.9 billion tons of wheat to 165 countries, while 30 countries exported 0.3 billion tons of rice to 48 countries (FAO 2025), highlighting the "thin" market for rice compared to wheat.

Results

City-specific food-miles and distance-sufficiency curve. To quantify the transport load of each commodity to each city, the food-miles was selected as the main metric. The food-miles is generally expressed in tons-kilometers (t km) and represents the distance transported multiplied by the mass of food item (NCAT 2008, Li et al. 2022). Using the global gridded maps of crop area and yield, population and road and vessel density, as well as the country-level data on trade matrix and per capita consumption of wheat and rice for food, we estimated global freight transport routes from production to consumption areas (Fig. 1 a) and the mass of the crops transported per route at the 30-arcmin resolution (~55 km at the equator). The distance transported and the mass of the crops transported, both estimated per route, were used to calculate the food-miles and its derivative, the distance-sufficiency curve, for each city (see **Methods**).

Freight transport routes estimated by the Dijkstra algorithm were more plausible than those derived by the great-circle algorithm if the fact that freight transport generally uses road and sea routes, but not air routes, was taken into account (Supplementary Fig. 1). The distance-sufficiency curves derived here revealed substantial variations between the cities. We therefore classified them into three groups using the clustering technique for characterization purposes. The results showed that more than two-thirds of the cities had an S-shaped curve, or a gamma (Γ)-shaped curve in an extreme case (Cluster 1 for both wheat and rice in Fig. 1 b, Supplementary Fig. 2). This shape of the distance-sufficiency curve indicates a relatively short distance (<10^3 km) to satisfy the city's food demand, and mainly due to the contributions from domestic production and/or imports from neighboring countries. The second distinct group of the cities exhibited a vertically mirrored L (⅃)-shaped curve, indicating a high dependence on imports from a limited number of distant exporting countries (Cluster 3 for wheat and Cluster 2 for rice). This group also included a relatively liner shape, as seen around the diagonal line in the distance-sufficiency space. The dependence of imports from multiple exporting countries, both neighboring and distant, explains this shape. The remaining group had an L-shaped curve rotated 90° counterclockwise (⎵), indicating that current domestic production and imports are insufficient to meet the city's food demand (Cluster 2 for wheat and Cluster 3 for rice). Since clustering was performed for each commodity, the cluster numbers are not the same, even though the shapes of the distance-sufficiency curves are similar between the commodities

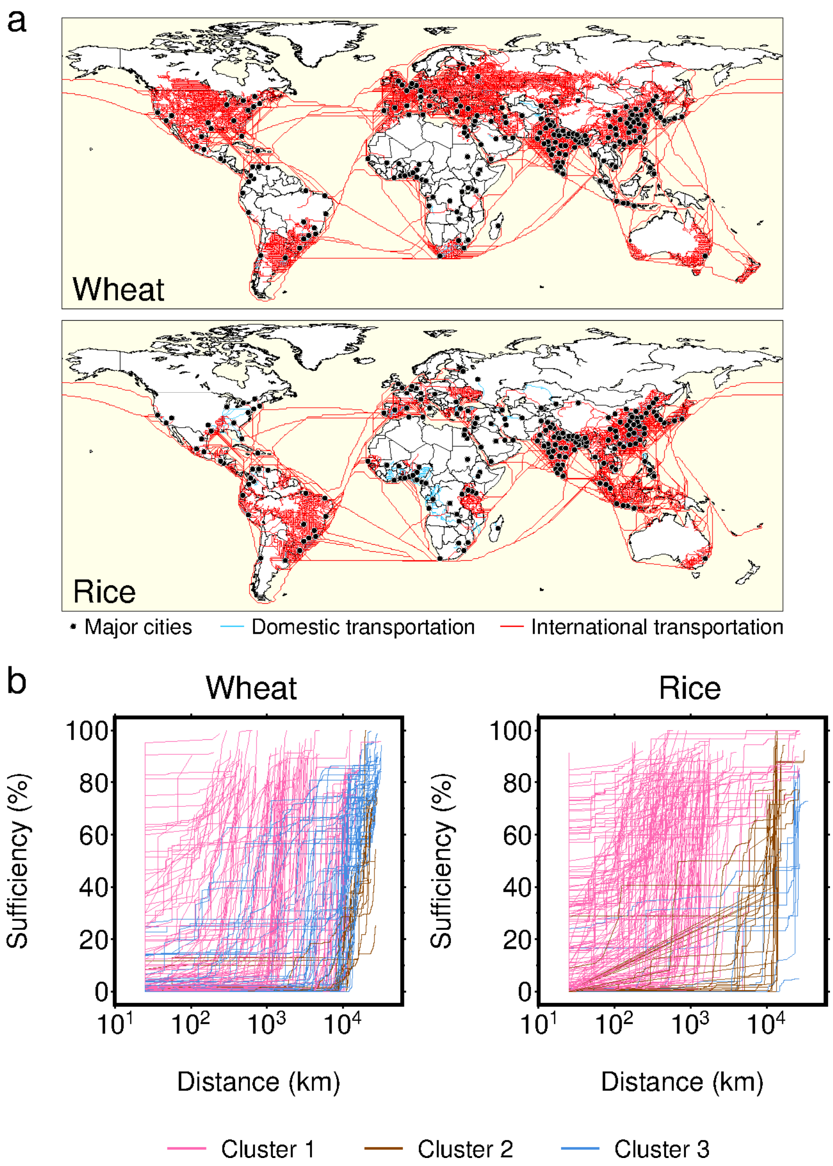

Fig. 1. Estimated freight transport routes and distance-sufficiency curves. a. Current wheat and rice transport routes from the production areas to the 208 major cities, estimated using the Dijkstra algorithm. A distinction is made between the estimated domestic and international transports. **b**. The city-specific distance-sufficiency curve, showing the response of wheat and rice sufficiency for food consumption as a function of the distance from the production area to the city. The cities are classified into three groups in terms of food-miles using the complete linkage clustering method.

Comparisons in current food-miles between cities and crops. The distance-sufficiency curves revealed the characteristics of each city and commodity in terms of food-miles. We described some examples below for explanatory purposes. One example is that, in Singapore, the distance-sufficiency curve is relatively more S-shaped for rice compared to wheat (Fig. 2 a). Rice consumed in the city comes mainly from Asian countries (India, Vietnam, Thailand, Cambodia, Japan and Pakistan), while wheat comes from Oceanic and North American countries (Australia, the United States, Canada), with the exception of Malaysia. This contrast explains the different shapes of the distance-sufficiency curves between the commodities. Another example is that the wheat distance-sufficiency curve for Singapore is more gradual and smoothed, while that for Tokyo is steeper and more zigzagged. Tokyo's dependence on a small number of distant trading partner countries explains this feature of the curve—99.9% of wheat imported by Japan in 2023 came from only three countries: the United States (38.6%), Canada (38.4%) and Australia (22.9%). In contrast, a major portion of wheat consumed in Singapore came from the trading partners which are geographically close to the city—Australia (57.9%) and Malaysia (1.4%), compared to the United States (23.5%) and Canada (16.8%). This contributes to make the curve relatively gradual and smooth. As storage is not taken into account in this study, it is thought to be the reason why Singapore's sufficiency does not reach 100%.

In Western Europe, 10 of the 13 cities considered in this study (Barcelona, Duesseldorf, Lisboa, London, Madrid, Manchester, Milano, Paris, Stuttgart and Wien) achieved 70% sufficiency within 10,000 km (Fig. 2 b, Supplementary Fig. 3). The remaining cities were Amsterdam, Brussels and Napoli, which required an average of 16,542 km to reach the sufficiency level. In contrast, of the 30 cities in Sub-Saharan Africa, only four (Addis Ababa, Dakar, Shashemene and Cape Town) achieved 70% sufficiency within 10,000 km for wheat. Although wheat is not necessarily a staple cereal in Africa, this difference highlighted that food procurement in many Sub-Saharan African cities is characterized by longer food-miles than in Western European cities and therefore less robust to shocks during freight transport.

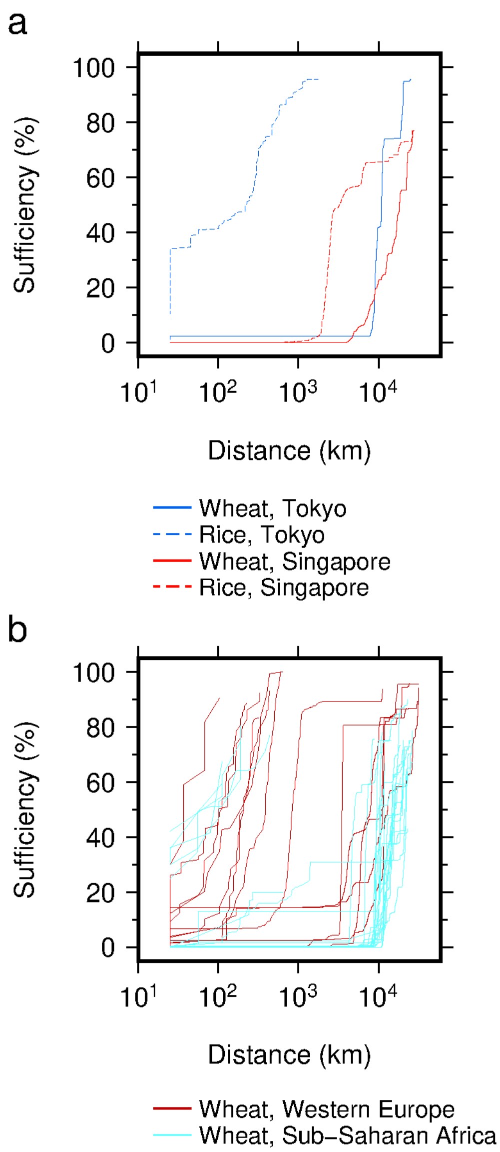

Fig. 2. Different distance-sufficiency curves characterizing food-miles. a. Comparison between wheat and rice for Singapore and between Singapore and Tokyo for wheat. **b**. Comparison between Sub-Saharan African and Western Europen cities for wheat.

Projected changes in food-miles. The food-miles for 2050 were projected based on four different scenarios of the impact of climate change on crop yields. The projected changes in demographics and crop area based on the "meddle-of-the-road" Shared Socio-economic Pathways (SSP2) were commonly considered across the different yield scenarios. Two population datasets were used as the different representation of the future population scenario. The yield scenarios were based on the ensemble mean projections of 12 global gridded crop models (GGCMs) with climate inputs from two global climate models (MPI-ESM1-2-HR and MRI-ESM2-0) forced with low and high emission scenarios (referred to as SSP126 and SSP585, respectively). We compared the food-miles impact of changes in mean climate for 2050 with that induced by the El Niño-Southern Oscillation (ENSO), to give readers a sense of how large the projected changes are relative to the variations in food-miles due to current natural climate variability. To do this, we used the mean yields over the El Niño (La Niña) years, relative to neutral years, for the current climate, as well as the mean yields over the ENSO neutral years for the future climate, both calculated using the multi-GGCM ensemble mean yield projections and the climate models' monthly sea surface temperature (**Methods**).

The projected population decreased in East Asia and Europe, but increased in many parts of the world for both datasets (Supplementary Fig. 4). Under the SSP2 socio-economic scenario, the crop area was expected to remain unchanged or decrease. Particularly, the noticeable decreases were in China, India, Canada and Brazil for wheat and in China, India, Thailand and Cambodia for rice (Supplementary Fig. 5). Compared to population and crop area, the impact of climate change on yields was projected to be more complex in terms of geographic patterns. The wheat yield was projected to increase in Europe but decrease in India under the climate projection derived from the MPI-ESM1-2-HR climate model, regardless of the emission scenarios (SSP126 and SSP585) (Supplementary Fig. 6). Under different climate projection derived from the MRI-ESM2-0 climate model, the wheat yield would decrease in many parts of Europe, Australia and Argentina for both SSP126 and SSP585. For rice, although both signs of change were found, the yield decrease was relatively widespread in Asia (Supplementary Fig. 7). This trend was relatively consistent across the different climate models and emission scenarios.

The projected food-miles could be greater than the current maximum or smaller than the current minimum, when compared to the current min-max range of food-miles associated with ENSO in the historical period. In 68 of the 208 cities, it was projected that the food-miles required to achieve 70% sufficiency of the city's wheat demand (FM70) in 2050 would be greater than the current maximum FM70 associated with ENSO (Fig. 3, Supplementary Fig. 8). Here, we set the threshold at 70% to avoid extremely long food-miles due to small amounts of imports from distant countries, and also to take into account the fact that nearly 30% of food is lost between harvest and consumption (FAO 2011). However, in 61 cities, the wheat FM70 would be smaller than the ENSO-induced current minimum FM70. The remaining 79 cities were projected to fall within the current min-max range. For rice, the FM70 for 2050 was projected to exceed the ENSO-induced maximum for 85 cities, while it would fall below the ENSO-induced minimum for 54 cities, with 69 cities falling within the current min-max ranges.

Increases in FM70 were found in many more cities for rice than for wheat. While rice area and yield were expected to decrease in India, the country's population was projected to increase (Supplementary Fig. 4, Supplementary Fig. 5, Supplementary Fig. 7). As a result, the food-miles for rice were projected to increase in more Indian cities than for wheat (Fig. 3). However, decreases in FM70 for rice also appeared. Food-miles for rice in West African cities were projected to decrease or unchanged. As rice consumed in the cities was estimated to be transported domestically (Fig. 1 b), the projected yield increases in the region mainly explain this result (Supplementary Fig. 7).

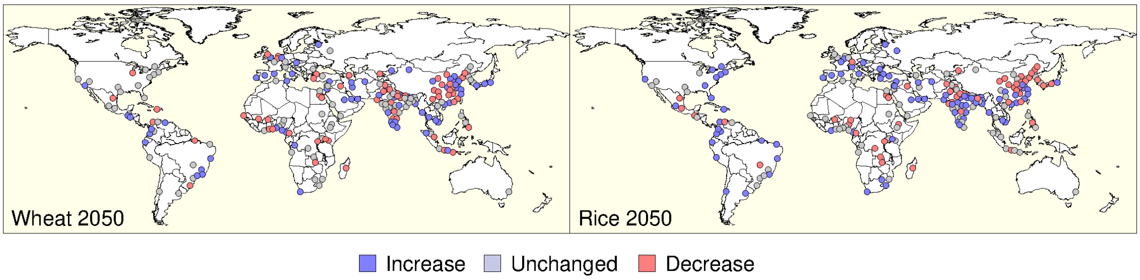

Fig. 4. Projected changes in wheat and rice food-miles for major cities in 2050. The median changes in the food-miles required to achieve 70% sufficiency (FM70) in 2050 are presented. The projected changes in FM70 are relative to the average FM70 over the ENSO neutral years in the current climate. The median values are derived based on six projections, consisting of two emission scenarios (SSP126 and SSP585), two climate models (MPI-ESM1-2-HR and MRI-ESM2-0) and two representations of the future population scenario (the JO and MY datasets). Only the data in the ENSO neutral years are used for the future climate.

Relative contributions to uncertainty in projected food-miles. To understand the relative contributions of main sources of uncertainty, we performed analysis of variance (ANOVA) on the projected FM70 from one city to another. There was a common trend across the commodities that the different representations of the future population scenario (i.e., the JO and MY datasets) explained a dominant proportion (86.3–89.3%) of the uncertainty in the projected FM70 (Supplementary Fig. 9). The climate models and the emission scenarios were then identified as the second (5.3–5.7%) and third (2.2–4.0%) contributing sources, respectively. The finding that the different representations of the future population scenario are the main source of uncertainty makes intuitive sense, as the population determines the level of food demand in the city. The relatively limited contribution of the emission scenarios is understandable, as this study analyzes the mid-century where the increases in CO_2 concentration and resulting climate change, as well as the climate impact on yield, are relatively smaller than at the late century. However, the yield projections used here did not take into account yield improvements associated with future agricultural research and development. Consideration of future technology and management scenarios may change the result of the uncertainty analysis from that presented here.

Discussion

The food-miles estimated using the Dijkstra algorithm with the road and vessel density map presented in this study provide a more plausible representation of freight transport routes than the great-circle algorithm which is similar to air transport routes (Supplementary Fig. 1). Cereals are transported by road and sea, but rarely by air (Li et al. 2022). The difference between the two algorithms is particularly noticeable when freight transport routes pass through canals or straits, although the difference is relatively small when crossing the ocean. In addition, the grid-wise estimates of freight transport routes allow the distance-sufficiency curve to be derived for each city, and this approach is applicable to cities around the world. These features represent a notable improvement in the study of food miles. Importantly, city-specific food-miles need to be calculated with global geospatial data, as demonstrated in this study, because food procurement for cities is largely dependent on the globally interconnected food trade. The distance-sufficiency curve provides a means of investigating the effect of specific interventions on food procurement for each city in future research. Interventions may include reorganizing crop area, building new roads, changing trading partner countries, or placing storage facilities. Some of these have been studied (Beyer et al. 2022, Schneider et al. 2022), but none of the existing studies include global freight transport or transport loads to cities.

Comparisons between commodities and cities provide some insights into how to make food procurement for cities more robust. Under the current conditions of crop area and yields, population and freight transport routes, the distance-sufficiency curve for rice is S-shaped in many more cities than for wheat. Rice production areas are concentrated in Asia. This fact contributes relatively short food-miles for rice in the Asian cities, even if rice consumed in these cities is imported from neighboring countries. Relying on a crop that is abundant in domestic and neighboring production areas as a staple cereal is a good way to feed cities, as many Asian cities do with rice. The same is applied to the European and North American cities with wheat. Nevertheless, the difference in food-miles for wheat between Singapore and Tokyo leads to the idea that importing from a range of exporting countries, including both near and far and both major and minor, is considered a good practice to increase the robustness of food procurement.

Food procurement is affected by natural climate variability, such as ENSO, negatively or positively, depending on the cities and commodities through good or bad harvests in domestic production area and exporting countries (Anderson et al. 2023). Therefore, the impact of current natural climate variability provides a metric for understanding the magnitude of projected changes in food-miles for cities. The results indicate that the projected food-miles could vary by city and commodity, with the magnitude exceeding the range caused by current natural climate variability. This finding implies that, in principle, countermeasures for robust food procurement, including planning, need to be taken city by city. For example, an alliance of cities for joint procurement and storage may be beneficial, but the similarities and differences in the shape of the distance-sufficiency curve between cities need to be taken into account in risk diversification.

This study has a few limitations. First, river and rail transports are not considered. River transport is affected by low water levels and the length of ice season (Fukś et al. 2023). The droughts that hit the Missouri River in 2022 (National Integrated Drought Information System 2022) and the Panama Canal in 2023 (World Weather Attribution 2024) are notable examples. For rail transport, thermal expansion of rails leading to service delays or cancellations is an emerging concern (Palin et al. 2021, The Japan Times 2024). Second, road and sea routes would change in the coming decades. Projected economic development would expand road networks (Meijer et al. 2018). The availability of the Northern Sea Route in a warmer climate could alter sea routes between Europe and Asia (Nikkei Asia 2024). All of the above may lead to different results from those presented in this study. Last, food-miles may vary by season, as harvests in the northern and southern hemispheres differ by half a year, and as rainy season crops are harvested several months after the end of dry season. Storage infrastructure need to be taken into account when estimating realistic seasonal food-miles for cities.

Online Methods

Major cities. We studied world's 208 major cities (Supplementary Fig. 3, Supplementary

Data 1). For the identification of the major cities, we used the WorldPop global gridded map of population counts in 2010 (WorldPop 2024). The data was first aggregated from the 30-arcsec resolution (~1 km at the equator) to 30-arcmin resolution (~55 km). Land grid cells with a population greater than 2 million (M) were identified. Populated grid cells (≥ 2M) within 200 kilometers of the identified populated grid cell were merged to form a single city. Less populated grid cells (< 2M) were not associated with the identified cities. Therefore, each major city studied in this study consisted of one or more grid cells with >2 M people. The population of the studied cities varied from 2 M (ex. Fukuoka, Japan) to 121.6 M (Dhaka, Bangladesh) with median of 5.3 M (ex. Napoli, Italy). The population-weighted average longitude and latitude were used as the location of the city.

We used two gridded population scenarios for 2050, referred to as the JO (Jones and O'Neill 2016) and MY datasets (Murakami and Yamagata 2019). The data were spatially aggregated to the 30-arcmin resolution when necessary. The combination of the populated grid cells associated with each major city, as determined by the WorldPop data, was left unchanged for the future period. This means that while population changes within currently populated grid cells due to further urban sprawl and decay are taken into account, the expansion or emergence of a city into neighboring grid cells that are currently less populated is not. However, the results of this study are unlikely to be affected by this omission, as a relatively coarse grid size of 30-arcmin is used.

Crop yields and areas. Crop yield and harvested area are key information to characterize the geographic distribution of crop production. We used the global map of average yield and area of 2009–2011 obtained from the SPAM2010 dataset (Yu et al. 2020) as the baseline.

For future yield scenarios, the multi-GGCM ensemble mean yield projections (Jägermeyr et al. 2021, Jägermeyr et al. 2024) were used. As the original dataset includes percentage changes in yields relative to the 1983–2013 baseline, the harmonization was done to combine with the SPAM2010 yields. Although yield projections under five GCMs are available in the dataset, we selected the two GCMs (MPI-ESM1-2-HR and MRI-ESM2-0) for this study due to the computational burden of calculating global freight transport routes. The two GCMs have an intermediate equilibrium climate sensitivity (ECS) of 2.98–3.15 °C compared to the remaining three GCMs (3.90–5.34 °C). ECS is the change in global surface temperature, relative to pre-industrial levels, when the atmospheric CO_2 concentration doubles from 280 to 560 ppm and the Earth's climate reaches a new equilibrium state. Furthermore, we made distinction between El Niño, La Niña, and neutral years using the GCM-simulated sea surface temperature. Then the mean yields for each phase of ENSO for 2010 and 2050 were calculated using the data for the 1982–2020 and 2035–2064 period, respectively (Harrington-Tsunogai et al. 2025).

For the wheat and rice harvested areas in 2050, we used the global gridded land-use data under SSP2 socio-economic pathway with the baseline climate mitigation scenario (Fujimori et al. 2018, NIES 2018). This dataset is derived by using an integrated assessment model AIM/CGE (the Asian-Pacific Integrated Model/Computable General Equilibrium) with a spatial land-use disaggregation module called AIM/PLUM (the integration Platform for Land-Use and environmental Modelling) (Fujimori et al. 2012, Hasegawa et al. 2017).

Road and vessel density map. We used a global gridded map of road and vessel density to estimate the plausible land and sea transport routes from the production to consumption areas. To develop the map, the 5-arcmin resolution road density map (Meijer et al. 2018) and the 10-arcmin resolution vessel density map (Wu et al. 2017) were combined after aggregating them to the 30-arcmin resolution (Supplementary Fig. 10 a).

In the road density map, data were available for five categories—highways, primary roads, secondary roads, tertiary roads, and local roads—in units of kilometers per square meter. The latter three categories were combined and referred to as "the secondary roads", in relation to the known underestimation of local road density (Meijer et al. 2018) and for simplicity. We assumed that freight carriers use highways preferentially for long-distance transport, followed by primary roads, and secondary roads if no other options are available. For this, each 30-arcmin land grid cell was assigned to either of four categories, "highways", "primary roads", "secondary roads" and "no road available", depending on the presence of the higher category levels.

The vessel density map provided data on the number of vessels per square kilometer per year (v). Using the 30-arcmin resolution map, we identified secondary and primary sea routes using the threshold of $12<\ln(v)<13$ for the former and $13\leq\ln(v)$ for the latter, where ln(v) is the natural logarithm of the annual vessel density. The remaining sea grid cells were classified to as "no shipping route is available" for simplicity. We ensured that sea routes passing through the Panama Canal, the Suez Canal, and the Straits of Gibraltar were available in the developed map (Supplementary Fig. 10 b).

Freight transport route estimation. Commodity transport routes were estimated using the global map of the road and vessel density described above. To do this, we assumed the average time required to transport one ton of freight one kilometer and the average capacity of the standard freight specific to the road and sea route categories (Supplementary Table 1). The road and sea route categories were then translated into the node and edge information to find the shortest paths between two locations using the Dijkstra algorithm (Dijkstra 1959).

The nodes represent the center of a 30-arcmin grid cell. The edges represent the distance between the centers of adjacent grid cells, which varies with latitude and route category. In the Dijkstra algorithm, the distance is expressed in hours per ton per kilometer and depends on the average speed and the average freight capacity specific to the route category. National borders and land-sea borders were also considered because of the time required for customs procedures and loading and unloading. This was done by assuming a very long distance in the calculation of the Dijkstra algorithm (Supplementary Table 1).

The number of nodes was 259,200, consisting of 720×360 longitude and latitude grid cells. The number of edges was 889,656, excluding grid cells without any road and sea routes and sea grid cells that do not reach a land grid cell within the 3,000 kilometers. We computed the shortest path and distance in kilometers for each non-overlapping pair of 47,799 land grid cells using the Dijkstra algorithm implemented in Python (Van Rossum and Drake 2009). This corresponds to 71% of the land grid cells with non-zero rice or wheat harvested area or population in 2010.

Food-miles estimation. Food-miles was computed crop by crop. Supplementary Fig. 11

illustrates the estimation procedure. The procedure mainly consists of the three components: the initial crop balance, domestic transport, and international transport. The domestic and international transports include iterations. The mathematical descriptions of the procedure are available in Supplementary Text 1.

Initial crop balance. For the target crop, the local (grid-cell) production was calculated by multiplying harvested area by yield. The local production was then divided by type of utilization, i.e., for export, domestic consumption for food, feed, processing, and other uses (non-food/industrial), as well as for seed and losses. This breakdown by type of utilization was based on the national average share of utilization in 2009–2011 (Ray et al. 2022). The local production allocated for domestic food consumption and export were transported domestically and internationally.

Domestic transport. For each country, we calculated the local (grid-cell) surplus and deficit of the target crop and updated them by iteration with a maximum mass of the crop transported per step. To do this, the food consumption was derived by multiplying the local population by the national per capita consumption of the crop for food. The difference between the food consumption (C) and the production allocated for domestic food consumption (S) was calculated. The per capita consumption of the crop for food was calculated from the national-level data on crop production, production share for domestic food consumption, and population (FAO 2024). A positive and a negative value of the difference (S–C) are referred to as the crop's surplus and deficit, respectively.

The production surplus in a grid cell was transported to the nearest deficit grid cell within the same country. The surplus and deficit conditions of the two grid cells were updated after the domestic transport. The nearest gird cell was calculated using the Dijkstra algorithm as described above. This domestic transport calculation was iterated from the largest surplus grid cell to the smallest surplus grid cell, with a maximum transported mass of the crop transported per step (1,000 tons). Grid cells with zero surplus or zero deficit were removed from the iteration. The domestic transport calculation was terminated when the national sum of the local deficits or local surpluses reached zero, or when the national sum of the local deficits remained unchanged between the current and the previous steps. In the calculation of the Dijkstra algorithm, we did not consider crop prices, but transport costs in units of hours per ton per kilometer (h/t/km) (Supplementary Table 1). Therefore, it is reasonable to assume that production surpluses in one grid cell are transported to the nearest deficit grid cell is reasonable, although this assumption may not be hold if the difference in crop price between cities is large.

International transport. Even after the domestic transport calculation was finished, surplus and deficit grid cells remain many parts of the world. To calculate the international transport, the local surpluses were removed as national stocks and the local production for export was taken as the initial condition. To account for actual food trade conditions, the local production for export described above was further multiplied by the national export share for each importing country. For this, FAO's detailed trade matrix data (FAO 2024) were used. The surplus in a grid cell of an exporting country was then transported to the nearest deficit grid cell of an importing country, with a maximum mass of the crop transported per step (1,000 tons). The international transport calculation was terminated when the global sum of the local surpluses or local deficits became zero, or when the global sum of the local deficits remained unchanged between the current and the previous steps.

Derivation of distance-sufficiency curve for the major cities. The major city studied in this study consists of one or more grid cells with 30-arcmin resolution. The calculation results of the crop transport were extracted when the deficit cells are part of the major city. For each major city, the results included the mass of the crop transported domestically or internationally and the transport routes from the surplus (production) grid cells to the deficit (urban) grid cells. Using the results, the food-miles was calculated for each route to the major city by multiplying the mass of the crop transported by the distance transported.

The results were then used to construct the distance-sufficiency curve (DSC). This graph shows the relationship between the distance transported and the cumulative mass of the crop transported, which is expressed as a percentage of the total consumption of the crop for food in the given city (referred to as the sufficiency rate). The DSC accumulates the mass of the crop transported along with the distance transported from near to far. In general, the smaller the maximum mass of the crop transported per step, the smoother the DSC curve. We compared some values and selected 1,000 tons as a sufficiently small value. However, a jump in the DSC curve occurs when the country in which the major city is located imports the crop from the distant exporting countries. For some cities in the importing countries, the distance that required to achieve 100% sufficiency dramatically increases due to relatively trivial mass of the crop imported. To avoid the unpreferable influences of trivial amount of import, the distance required to achieve 70% sufficiency rate is used as a measure to assess the impact on food-miles. This is a reasonable assumption as it is estimated that 30–40% of total food production is lost between harvest and consumption (FAO 2011).

Data availability

Data supporting the findings of this study are publicly available. The gridded population data is accessible at: doi:10.5258/SOTON/WP00647 (WorldPop for 2010), https://sedac.ciesin.columbia.edu/data/set/popdynamics-1-8th-pop-base-year-projection-ssp-2000-2100-rev01/data-download (JO for 2050) and https://github.com/Nowosad/global_population_and_gdp?tab=readme-ov-file (MY for 2050). The gridded crop area data is available at: https://doi.org/10.7910/DVN/PRFF8V (SPAM2010) and doi:10.18959/20180403.001 (AIM/PLUM for 2050). The global gridded crop model ensemble mean percentage yield change data is accessible at: doi:10.21981/1XJY-C362. The country annual detailed trade matrix data is from the FAO statistical database: https://www.fao.org/faostat/en/#home.

Code availability

A sample program to draw the current distance-sufficiency curves is available at https://doi.org/10.5281/zenodo.15208245.

References

1. *World Urbanization Prospects: The 2018 Revision (ST/ESA/SER.A/420)* (United Nations, Department of Economic and Social Affairs, Population Division, 2019). https://population.un.org/wup/assets/WUP2018-Report.pdf
2. Seto, K. C., Ramankutty, N. Hidden linkages between urbanization and food systems.

Science **352**, 943–945 (2016). doi:10.1126/science.aaf7439

3. Ruel, M. T., Garrett, J. L., Hawkes, C. & Cohen, M. J. The food, fuel, and financial crises affect the urban and rural poor disproportionately: a review of the evidence. *J Nutr.* **140**, 170S–6S (2010). doi:10.3945/jn.109.110791
4. Miller, S. J. et al. Telecoupled systems are rewired by risks. *Nat. Sustain.* **7**, 247–254 (2024). https://doi.org/10.1038/s41893-024-01273-2
5. Gomez, M. et al. Supply chain diversity buffers cities against food shocks. *Nature* **595**, 250–254 (2021). https://doi.org/10.1038/s41586-021-03621-0
6. Nóia Júnior, R. de S. et al. Needed global wheat stock and crop management in response to the war in Ukraine. *Glob. Food Secur.* **35**, 100662 (2022). https://doi.org/10.1016/j.gfs.2022.100662
7. Jägermeyr, J. et al. Climate impacts on global agriculture emerge earlier in new generation of climate and crop models. *Nat. Food* **2**, 873–885 (2021). https://doi.org/10.1038/s43016-021-00400-y
8. Hasegawa, T., Wakatsuki, H. & Nelson, G. C. Evidence for and projection of multi-breadbasket failure caused by climate change. *Curr. Opin. Environ. Sustain.* **58**, 101217 (2022). https://doi.org/10.1016/j.cosust.2022.101217
9. Chen, X., Anderson, W., You, L. & Pope, E. Observed trends in multiple breadbasket yield shocks. *Environ. Res. Lett.* **19**, 104005 (2024). https://dx.doi.org/10.1088/1748-9326/ad7040
10. Zabel, F., Knüttel, M. & Poschlod, B. CropSuite – A comprehensive open-source crop suitability model considering climate variability for climate impact assessment. *EGUsphere* [preprint] (2024). https://doi.org/10.5194/egusphere-2024-2526
11. Zhang, T. et al. Increased wheat price spikes and larger economic inequality with 2 °C global warming. *One Earth* **5**, 907–916 (2022). https://doi.org/10.1016/j.oneear.2022.07.004
12. Tuholske, C. et al. A framework to link climate change, food security, and migration: unpacking the agricultural pathway. *Popul Environ* **46**, 8 (2024). https://doi.org/10.1007/s11111-024-00446-7
13. Dodman, D. et al. *Cities, Settlements and Key Infrastructure*. in *Climate Change 2022: Impacts, Adaptation and Vulnerability* (eds Pörtner, H.-O. et al.) Ch. 6 (Cambridge University Press, 2022). doi:10.1017/9781009325844.008
14. d'Amour, C. B., Weston, A. International trade and the stability of food supplies in the Global South. *Environ Res Lett* **15**, 074005 (2020). https://dx.doi.org/10.1088/1748-9326/ab832f
15. Xia, L. et al. Global food insecurity and famine from reduced crop, marine fishery and livestock production due to climate disruption from nuclear war soot injection. *Nat Food* **3**, 586–596 (2022). https://doi.org/10.1038/s43016-022-00573-0
16. *Ten things you should know about maize and wheat* (International Maize and Wheat Improvement Center (CIMMYT), 2019). https://www.cimmyt.org/news/ten-things-you-should-know-about-maize-and-wheat/
17. *2023 Annual Report* (International Rice Research Institute (IRRI), 2023). http://books.irri.org/AR2023_content.pdf
18. *FAOSTAT – Trade* (FAO, 2025). https://www.fao.org/faostat/en/#data/TCL
19. *Food Miles: Background and Marketing* (National Center for Appropriate

Technology (NCAT), 2008). https://attradev.ncat.org/wp-content/uploads/2022/06/foodmiles.pdf

20. Li, M. et al. Global food-miles account for nearly 20% of total food-systems emissions. *Nat. Food* **3**, 445–453 (2022). https://doi.org/10.1038/s43016-022-00531-w
21. *Global food losses and food waste – Extent, causes and prevention* (FAO, 2011). https://www.fao.org/4/mb060e/mb060e00.pdf
22. Beyer, R.M., Hua, F., Martin, P.A. et al. Relocating croplands could drastically reduce the environmental impacts of global food production. *Commun Earth Environ* **3**, 49 (2022). https://doi.org/10.1038/s43247-022-00360-6
23. Schneider, J. M. et al. Global cropland could be almost halved: Assessment of land saving potentials under different strategies and implications for agricultural markets. *PLoS ONE* **17**, e0263063 (2022). https://doi.org/10.1371/journal.pone.0263063
24. Anderson, W. et al. Climate variability and simultaneous breadbasket yield shocks as observed in long-term yield records. *Agric. For. Meteorol.* **331**, 109321 (2023). https://doi.org/10.1016/j.agrformet.2023.109321
25. Fukś, M. Changes in river ice cover in the context of climate change and dam impacts: a review. *Aquat. Sci.* **85**, 113 (2023). https://doi.org/10.1007/s00027-023-01011-4
26. *Drought Status Update for the Midwest and Missouri River Basin* (National Integrated Drought Information System, 2022). https://www.drought.gov/drought-status-updates/drought-status-update-midwest-and-missouri-river-basin-10-25-22
27. *Low water levels in Panama Canal due to increasing demand exacerbated by El Niño event* (World Weather Attribution, 2024). https://www.worldweatherattribution.org/low-water-levels-in-panama-canal-due-to-increasing-demand-exacerbated-by-el-nino-event/
28. Palin, E. J., Oslakovic, I. S., Gavin, K. & Quinn, A. Implications of climate change for railway infrastructure. *WIREs Clim. Change* **12**, e728 (2021). https://doi.org/10.1002/wcc.728
29. *Japan's searing summer heat is warping railway tracks more often* (The Japan Times, 2024). https://www.japantimes.co.jp/news/2024/08/15/japan/heat-warping-railway-tracks/
30. Meijer, J. R., Huijbregts, M. A. J., Schotten, K. C. G. J. & Schipper, A. M. Global patterns of current and future road infrastructure. *Environ. Res. Lett.* **13**, 064006 (2018). https://dx.doi.org/10.1088/1748-9326/aabd42
31. *How The Northern Sea Routes Will Change The World's Major Traffic Flows* (Nikkei Asia, 2024). https://vdata.nikkei.com/en/newsgraphics/northern-sea-route/
32. *The spatial distribution of population in 2010* (WorldPop, 2024). doi:10.5258/SOTON/WP00647
33. Jones, B. & O'Neill, B. C. Spatially explicit global population scenarios consistent with the Shared Socioeconomic Pathways. *Environ. Res. Lett.* **11**, 084003 (2016). https://dx.doi.org/10.1088/1748-9326/11/8/084003
34. Murakami, D. & Yamagata, Y. Estimation of gridded population and GDP scenarios with spatially explicit statistical downscaling. *Sustain.* **11**, 2106 (2019). https://doi.org/10.3390/su11072106
35. Yu, Q. et al. A cultivated planet in 2010 – Part 2: The global gridded agricultural-

production maps. *Earth Syst. Sci. Data* **12**, 3545–3572 (2020) https://doi.org/10.5194/essd-12-3545-2020

36. Jägermeyr, J. et al. *AgMIP Data Aggregator Tool* (2024). doi:10.21981/1XJY-C362
37. Fujimori, S. et al. Gridded emissions and land-use data for 2005–2100 under diverse socioeconomic and climate mitigation scenarios. *Sci. Data* **5**, 180210 (2018). https://doi.org/10.1038/sdata.2018.210
38. *AIM-SSP/RCP Gridded Emissions and Land-use data* (National Institute for Environmental Studies (NIES), 2018). doi:10.18959/20180403.001
39. Harrington-Tsunogai, J. et al. ENSO impacts on global yields of major crops projected by a climate-crop model ensemble. *Jxiv* (Preprint) (2025). https://doi.org/10.51094/jxiv.1159
40. Fujimori, S., Masui, T. & Matsuoka, Y. AIM/CGE [Basic] Manual; Version 2012-01 (Center for Social and Environmental Systems Research, NIES, 2012). https://www.nies.go.jp/social/publications/dp/pdf/2012-01.pdf
41. Hasegawa, T., Fujimori, S., Ito, A., Takahashi, K. & Masui, T. Global land-use allocation model linked to an integrated assessment model. *Sci. Total Environ.* **580**, 787–796 (2017). https://doi.org/10.1016/j.scitotenv.2016.12.025
42. Wu, L., Xu, Y., Wang, Q., Wang, F. & Xu, Z. Mapping global shipping density from AIS data. *J. Navig.* **70**, 67–81 (2017). https://doi.org/10.1017/S0373463316000345
43. Dijkstra, E. W. A note on two problems in connexion with graphs. *Numer. Math.* **1**, 269–271 (1959). https://doi.org/10.1007/BF01386390
44. Van Rossum, G. & Drake, F. L. *Python 3 Reference Manual* (CreateSpace, 2009).
45. Ray, D. K. et al. Crop harvests for direct food use insufficient to meet the UN's food security goal. *Nat. Food* **3**, 367–374 (2022). https://doi.org/10.1038/s43016-022-00504-z
46. *Detailed trade matrix* (FAO, 2025). https://www.fao.org/faostat/en/#data/TM

Acknowledgements

TI, TT, MH and HS were supported by the Environment Research and Technology Development Fund (Grant Number: JPMEERF23S21120) of the Environmental Restoration and Conservation Agency provided by the Ministry of the Environment of Japan. HS was supported by the Advanced Studies of Climate Change Projection (SENTAN, grant number: JPMXD0722680395) of the Ministry of Education, Culture, Sports, Science and Technology of Japan. TI and TT used the supercomputer of the Agriculture, Forestry and Fisheries Research Information Technology Center, Ministry of Agriculture, Forestry and Fisheries of Japan. TI thanks Lin Wu for sharing the vessel density map, John Harrington-Tsunogai and Yoshiko Higashikozono for support in data curation, and Yoshimitsu Masaki and Yuji Masutomi for support in computation.

Author contributions. TI conceptualized this study, developed methodology, conducted formal analysis and wrote the original manuscript. TT contributed to data interpretation and software. MH and HS contributed climate data curation. TH and SF contributed socio-economic data curation. All authors contributed to manuscript editing.

Competing interests

The authors declare no competing interests.

Additional information

Supplementary material accompanies this manuscript.

Supplementary Materials

The followings accompany this paper:

- Supplementary Data 1
- Supplementary Text 1
- Supplementary Table 1
- Supplementary Figures 1 to 11

Supplementary text 1.

Overview of the crop transport calculation. The procedure of calculating global crop transports consists of three components: the initial crop balance, domestic transport, and international transport. Each component is elaborated below.

Initial crop balance. The initial crop balance condition provides the starting point for the domestic transport. The crop balance is the difference between the production and consumption of the crop for food. On the one hand, the production of the crop for food consumption in the grid cell, $\mathrm{prod.food}_{g,c}$ (t), is calculated as:

$$\mathrm{prod.food}_{g,c} = \mathrm{yld}_{g,c} \times \mathrm{area}_{g,c} \times \mathrm{fr.food}_{i,c}$$

where the suffix *g*, *c* and *i* indicate the grid cell, the crop and the country, respectively, and $\mathrm{yld}_{g,c}$ is the yield of the crop in the grid cell (t/ha), $\mathrm{area}_{g,c}$ is the harvested area of the crop in the grid cell (ha), and $\mathrm{fr.food}_{i,c}$ is the crop's production share for food consumption in the country (fraction). On the other hand, the consumption of the crop for food in the grid cell, $\mathrm{cons}_{g,c}$ (t), is calculated as:

$$\mathrm{cons}_{g,c} = \mathrm{pop}_{g} \times \mathrm{cons.pc}_{i,c} / 1000$$

where pop_{g} is the population in the grid cell (persons) and $\mathrm{cons.pc}_{i,c}$ is the annual per capita consumption of the crop for food in the country (kg/person). The country annual per capita consumption of the crop for food, $\mathrm{cons.pc}_{i,c}$ (kg/person), is calculated as:

$$\mathrm{cons.pc}_{i,c} = [\ (\ \mathrm{yld}_{i,c} \times \mathrm{area}_{i,c} + \mathrm{impt}_{i,c} - \mathrm{expt}_{i,c}\ ) \times \mathrm{fr.food}_{i,c}\ ] / \mathrm{pop}_{i} \times 1000$$

where $\mathrm{yld}_{i,c}$ is the average yield of the crop in the country (t/ha), $\mathrm{area}_{i,c}$ is the total harvested area of the crop in the country (ha), $\mathrm{impt}_{i,c}$ is the annual mass of the crop imported by the country (t), $\mathrm{expt}_{i,c}$ is the annual mass of the crop exported by the country (t), $\mathrm{fr.food}_{i,c}$ is the crop's production share in the country for food consumption (fraction), and pop_{i} is the total population in the country (persons).

The balance of the crop between the production and consumption for food in the grid cell, $\mathrm{spdf}_{g,c}$ (t), is calculated as:

$$\mathrm{spdf}_{g,c} = \mathrm{prod.food}_{g,c} - \mathrm{cons}_{g,c}$$

A positive and a negative $\mathrm{spdf}_{g,c}$ value are referred to as the surplus and deficit of the crop for food consumption, respectively. The local crop transport within the grid cell is then calculated, assuming that the transported distance is the half of the grid interval (~28 km):

$$\mathrm{tp}_{gs\rightarrow gd,c} = \min(\ \mathrm{prod}_{g,c}, \mathrm{cons}_{g,c}\ )$$

where the suffix *gs* and *gd* are the surplus and deficit grid cells, respectively, and $\mathrm{tp}_{gs\rightarrow gd,c}$ is the crop transported locally from the surplus grid cell to the deficit grid cell (t). For the local transport, the surplus and deficit grid cells are the same (gs=gd).

Domestic transport. After the local transport, the domestic transport begins to fill the crop deficits for food consumption with the surpluses in the same country. For each country, the crop is transported from a surplus grid cell to the nearest deficit grid cell with a maximum transport mass per step of 1,000 tons:

$$\mathrm{tp}_{gs\rightarrow gd,c} = \min(\ \mathrm{spdf}_{gs,c}, |\mathrm{spdf}_{gd,c}|, 1000\ )$$

where $\mathrm{tp}_{gs\rightarrow gd,c}$ is the mass of the crop transported domestically (t), $\mathrm{spdf}_{gs,c}$ is the surplus in the grid cell where the crop is produced (t) and $|\mathrm{spdf}_{gd,c}|$ is the absolute value of the deficit in the grid cell where the crop is transported domestically (t). An absolute value of the deficit is used here because the transport mass is always positive or zero. The above equation leads to one of the following results. If both the surplus ($spdf_{gs,c}$) and the deficit ($|spdf_{gd,c}|$) are greater (>1000), then a maximum mass of the crop transported per step is set as the crop transported, i.e., $tp_{gs\rightarrow gd,c} = 1000$. If both the surplus ($spdf_{gs,c}$) and the deficit ($|spdf_{gd,c}|$) are smaller (≤1000), then the following rules apply – if the surplus is smaller than the absolute value of the deficit ($spdf_{gs,c} < |spdf_{gd,c}|$), then the crop transported is calculated as $tp_{gs\rightarrow gd,c} = spdf_{gs,c}$ and if the surplus is greater than or equal to the deficit ($spdf_{gs,c} \geq |spdf_{gd,c}|$), then the crop transported is calculated as $tp_{gs\rightarrow gd,c} = |spdf_{gd,c}|$. After determining the transported mass of the crop, the crop balance conditions for a pair of the surplus and deficit grid cells are updated:

$$spdf_{gs,c} = spdf_{gs,c} - tp_{gs\rightarrow gd,c} \text{ and } spdf_{gd,c} = spdf_{gd,c} + tp_{gs\rightarrow gd,c}.$$

The crop transport calculation described above for the country *i* is repeated until the sum of the national sum of the deficits or surpluses reached zero, or the national sum of the deficits remains unchanged between the current and the previous steps. This calculation is repeated for all countries.

International transport. After calculating the domestic transport, the surplus of the crop in the grid cells is considered as the stock in the country and eliminated from the international transport. In the international transport, for each country, the production of the crop for export in the grid cell, $prod.expt_{g,c}$ (t), is calculated as:

$$prod.expt_{g,c} = yld_{g,c} \times area_{g,c} \times fr.expt_{i,c}$$

where $yld_{g,c}$ is the yield of the crop in the grid cell (t/ha), $area_{g,c}$ is the harvested area of the crop in the grid cell (ha), and $fr.expt_{i,c}$ is the crop's production share for export in the country (fraction). The surplus of the crop in the grid cell is replaced with the production of the crop for export:

$$spdf_{g,c} = prod.expot_{g,c} \quad \text{if } spdf_{g,c} \geq 0.$$

The deficit of the crop in the grid cell remains the same:

$$spdf_{g,c} = spdf_{g,c} \quad \text{if } spdf_{g,c} < 0.$$

The crop transported from the surplus grid cell in an exporting country to a deficit grid cell in the importing country, $tp_{gs\rightarrow gd}$ (t), is calculated in the similar way as for the domestic transport calculation:

$$tp_{gs\rightarrow gd,c} = \min(\, spdf_{gs,c} \times fr.trade_{i,j},\ |spdf_{gd,c}|,\ 1000\,).$$

The only difference is that the export share of the exporting country *i* to the importing country *j*, $fr.trade_{i,j}$ (fraction), is taken into account by multiplying it by the surplus of the crop in the grid cell of the exporting country. Once the mass of the crop transported internationally is determined, the crop balance conditions are updated for the surplus in the grid cell of the exporting country and the deficit in the grid cell of the importing country, as in the domestic transport calculation:

$$spdf_{gs,c} = spdf_{gs,c} - tp_{gs\rightarrow gd,c} \text{ and } spdf_{gd,c} = spdf_{gd,c} + tp_{gs\rightarrow gd,c}.$$

The crop balance condition at the global level is then calculated. The global sum of the crop surpluses, $sum.sp_c$ (t), and the global sum of the crop deficits, $sum.df_c$ (t), are calculated. The international transport calculation is terminated when $sum.sp_c$ or $sum.df_c$ becomes zero, or when $sum.df_c$ remains unchanged between the current and the previous steps.

Supplementary Table 1. The settings related to distance used in the calculation of Dijkstra algorithm,

Road and shipping routes category	Average speed (km/h)	Average cargo capacity (t)	Distance used in Dijkstra algorithm (h/t/km)
Primary sea route	40	100	2.5×10^{-4}
Secondary sea route	40	50	5.0×10^{-4}
Highways	80	10	12.5×10^{-4}
Primary roads	50	5	40×10^{-4}
Secondary roads	30	2	167×10^{-4}
National or land-sea borders	5	10	200×10^{-4}
No road or shipping route is available	–	–	–

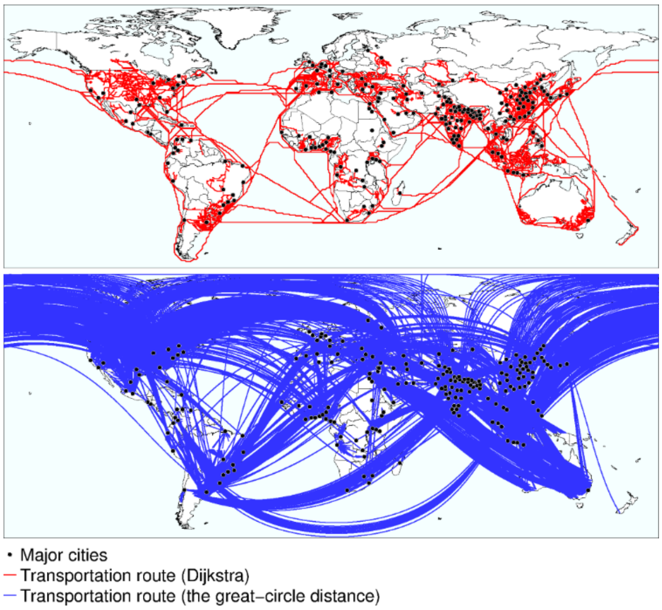

Supplementary Fig. 1. The shortest routes to the major cities estimated using the Dijkstra algorithm and great-circle distance algorithm.

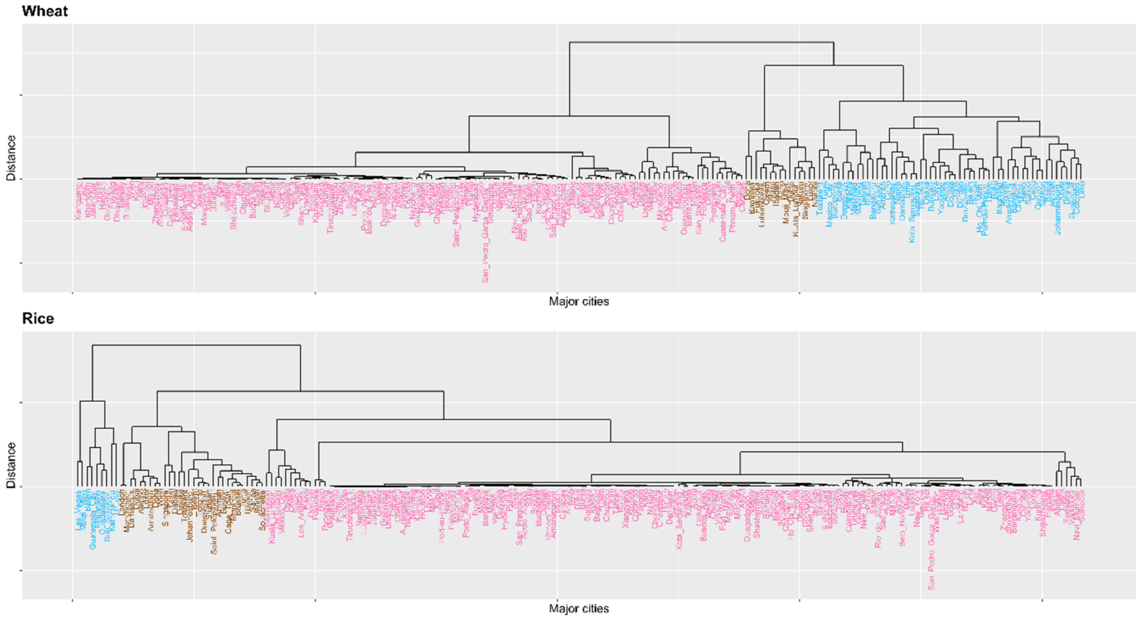

Supplementary Fig. 2. Dendrogram illustrating the clustering result. The 208 major cities are classified to three groups based on the current distance-sufficiency curves using the complete linkage clustering method in R.

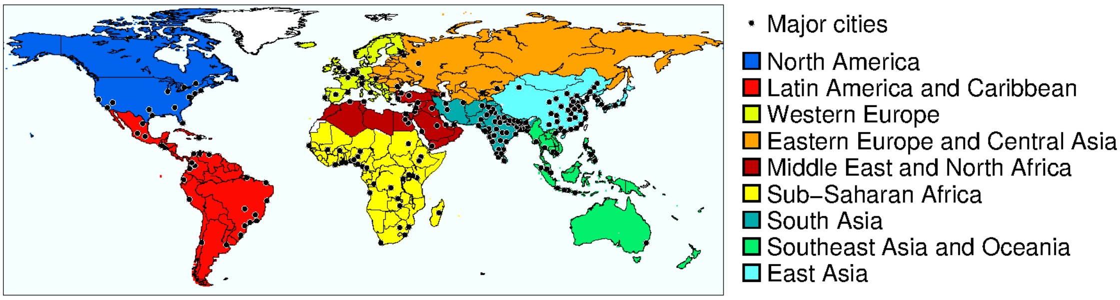

Supplementary Fig. 3. The 208 major cities of the world studied in this study. Colors indicate the classification by geographic region.

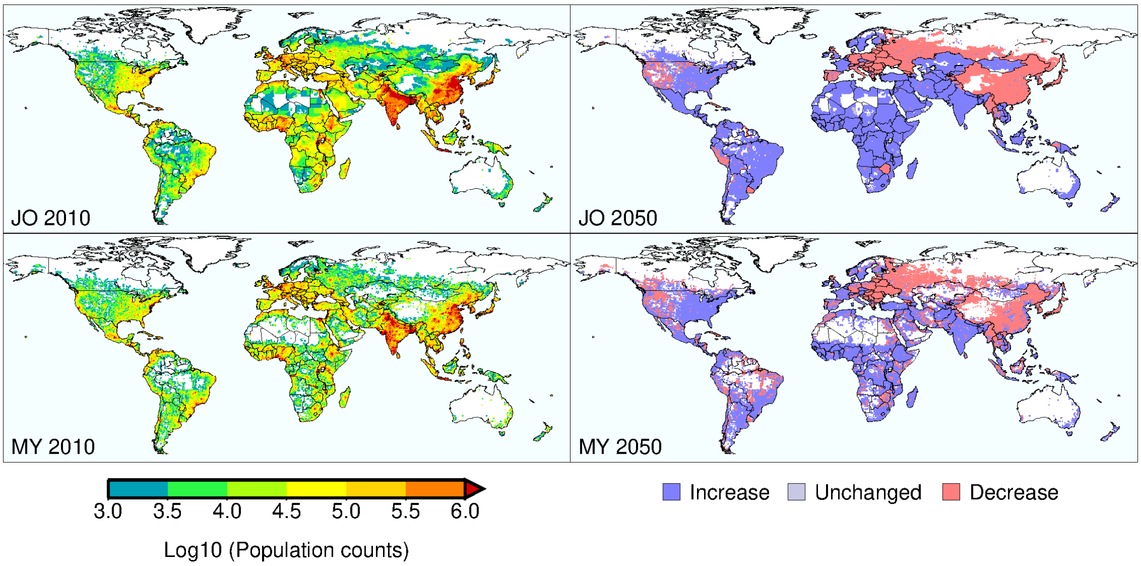

Supplementary Fig. 4. Geographic distribution of population in 2010 and projected change in 2050. The data presented here are obtained from two sources: Jones and O’Neill (2016) (JO) and Murakami and Yamagata (2019) (MY).

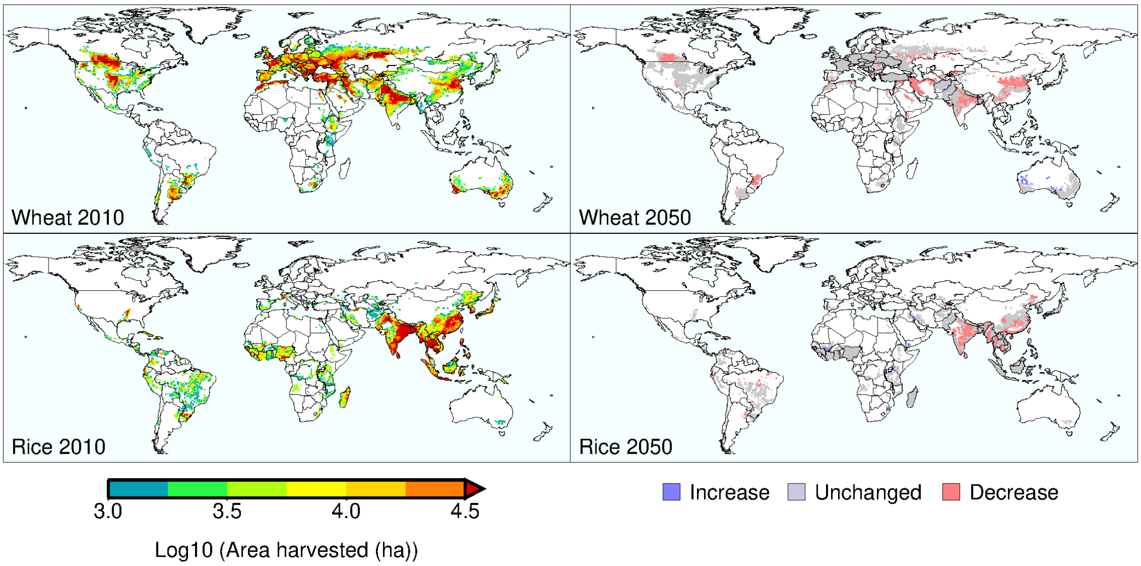

Supplementary Fig. 5. Geographic distribution of harvested area in 2010 and projected change in 2050 for wheat and rice. The projected data are based on the socioeconomic pathways SSP2 and obtained from NIES (2018).

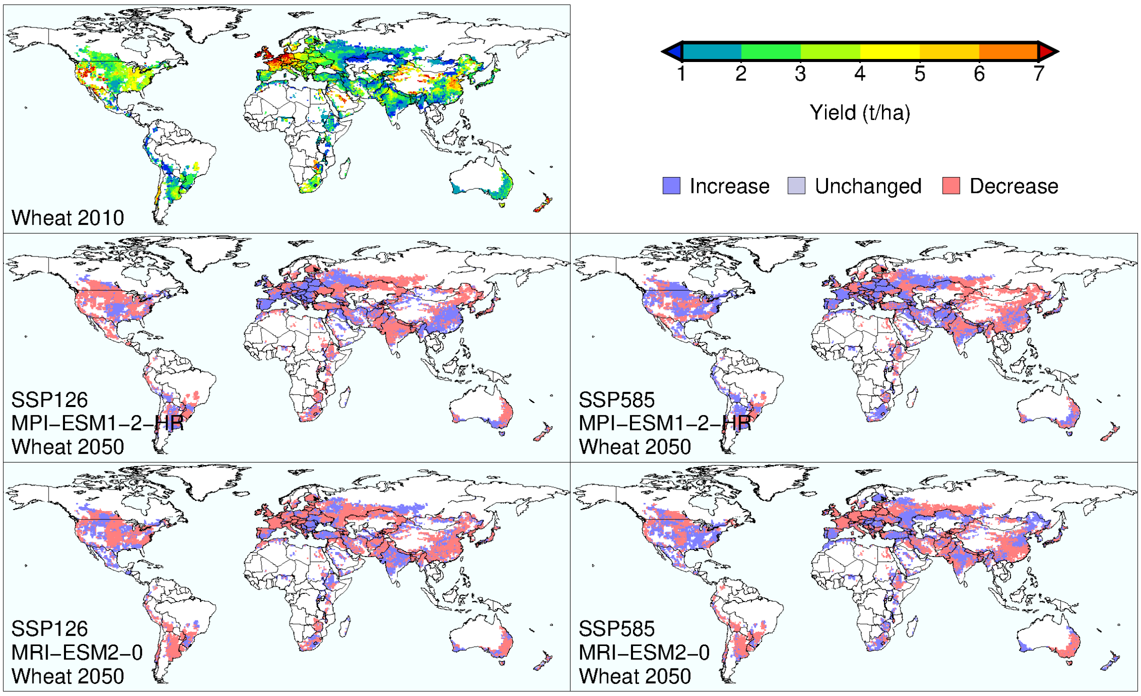

Supplementary Fig. 6. Geographic distribution of yield in 2010 and projected change in 2050 for wheat. The projected data are for ENSO neutral years and sourced from Jägermeyr et al. (2024) and Harrington-Tsunogai et al. (2025).

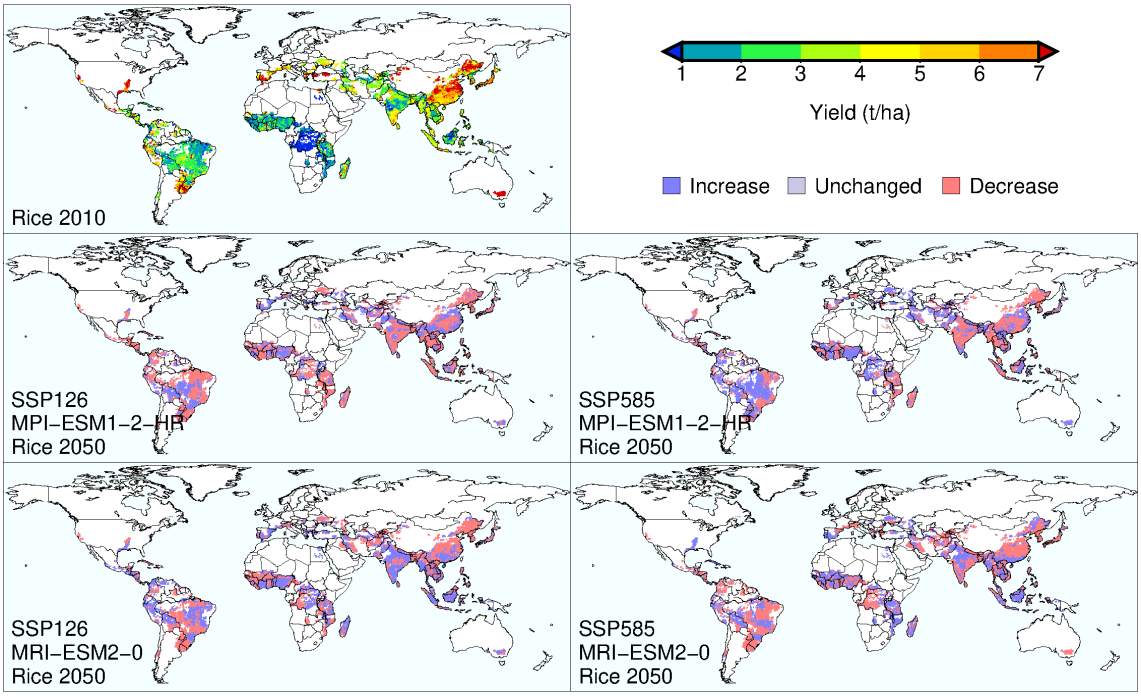

740 Supplementary Fig. 7. Same as Supplementary Fig. 6, but for rice.

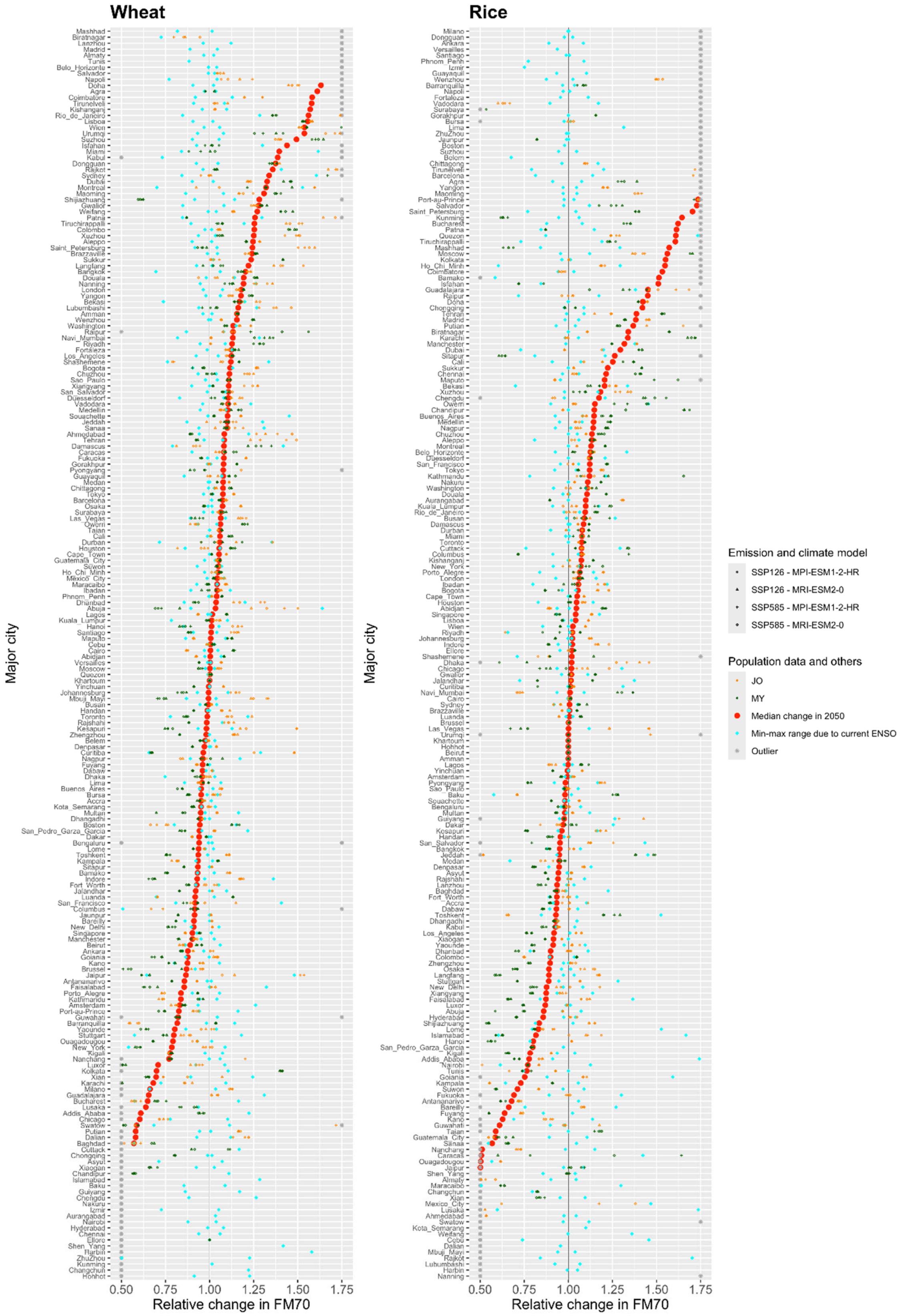

Supplementary Fig. 8. Projected changes in crop-specific FM70 for wheat and rice in 2050. The projected changes in FM70 are relative to the average FM70 over the ENSO neutral years in the current climate. Six projections are considered, consisting of two emission scenarios (SSP126 and SSP585), two climate models (MPI-ESM1-2-HR and MRI-ESM2-0) and two representations of the future population scenario (the JO and MY datasets). Only the data in the ENSO neutral years are used for the future climate. The ENSO-induced min-max range represents the variation in historical FM70 and relative to the average over the current ENSO neutral years.

751

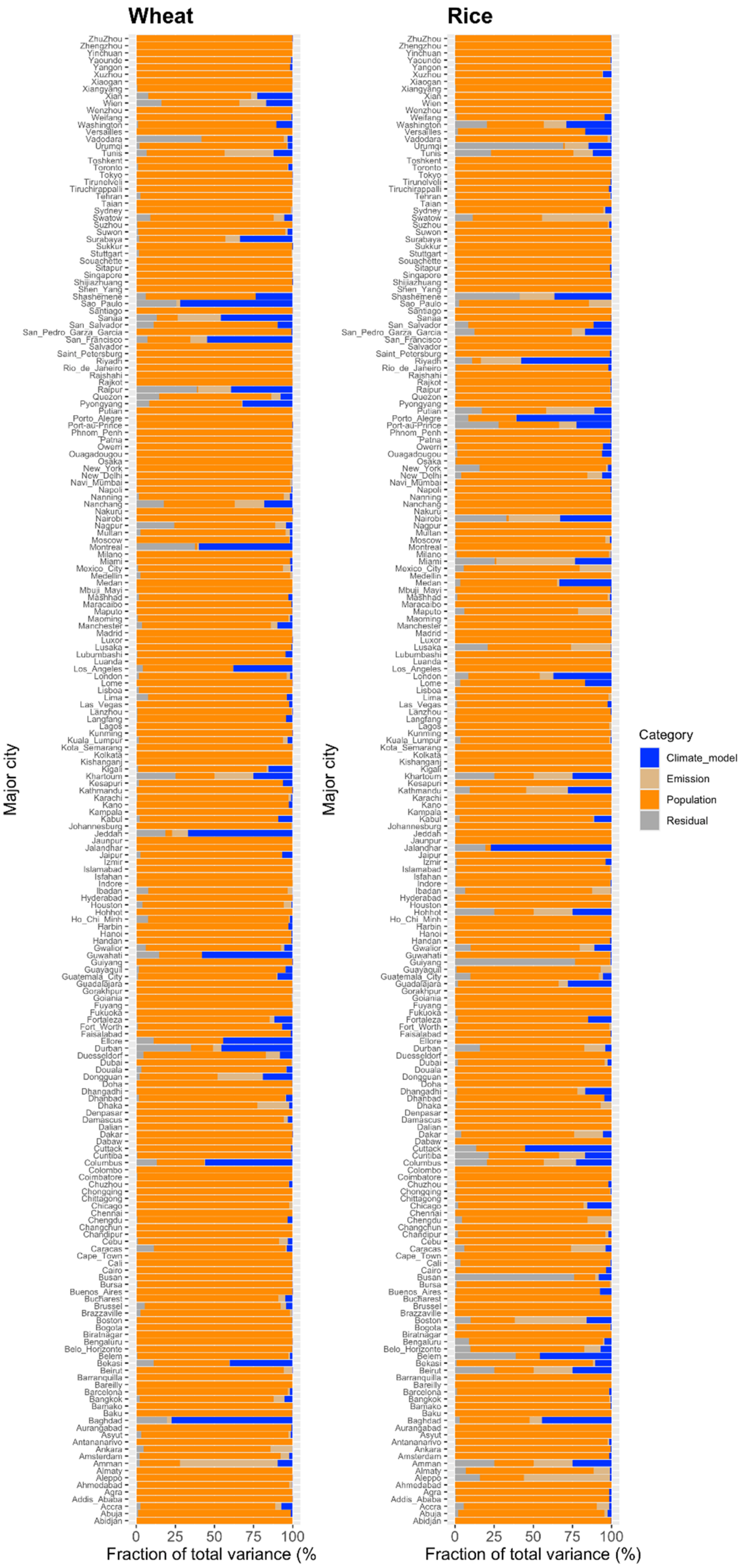

Wheat
Rice
Major city
Fraction of total variance (%
Fraction of total variance (%)
0
25
50
75
100
Category
Climate_model
Emission
Population
Residual

Supplementary Fig. 9. The relative contribution of each source of uncertainty in the projected change in FM70 for the 208 major cities in 2050. The fraction of total variance in the projected change in FM70 is explained by use of different population datasets, emission scenarios (RCP) and climate models (GCM). The residual indicates the remaining uncertainty which is not explained by the three sources of uncertainty.

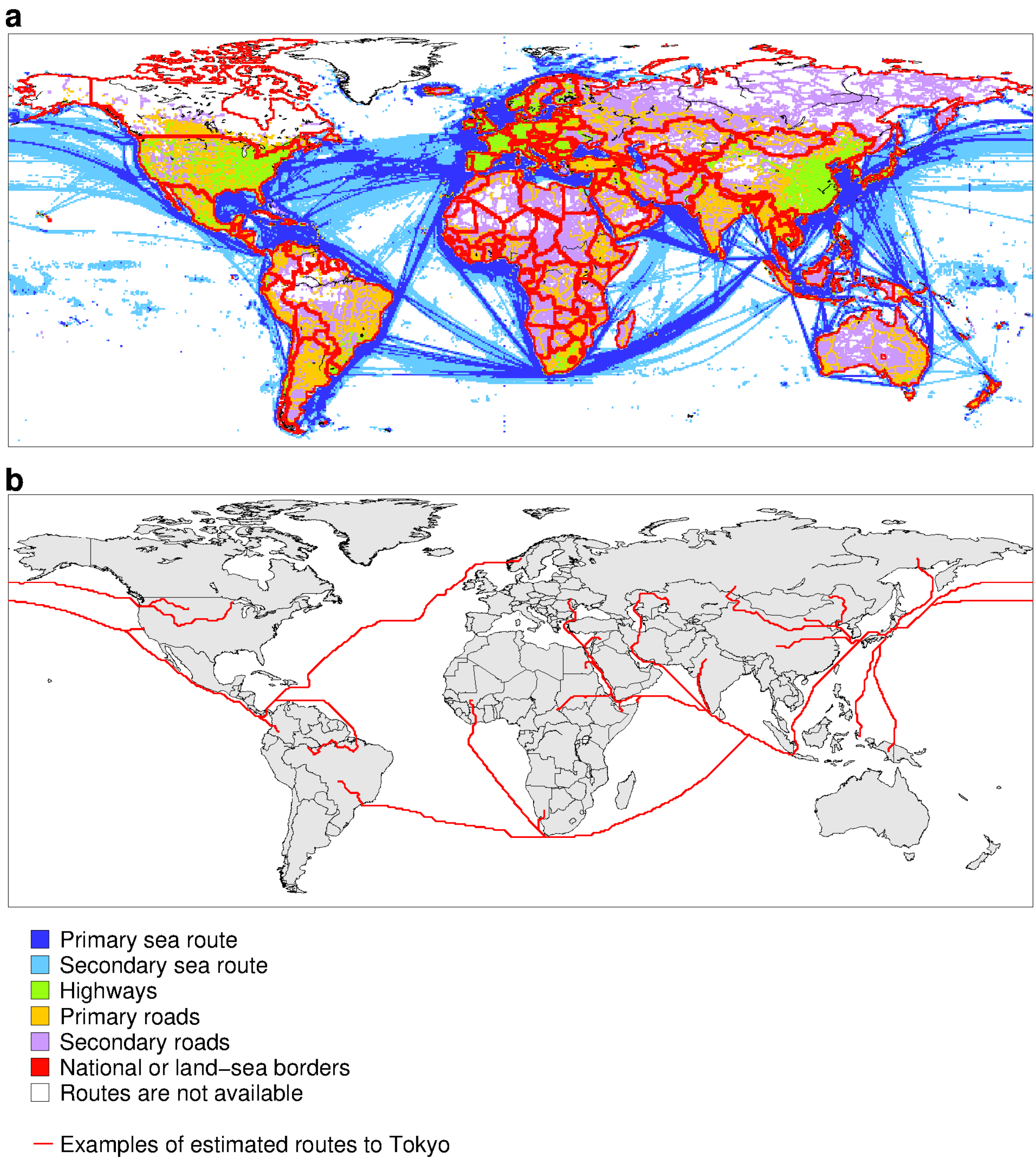

Supplementary Fig. 10. Global map of freight transport route categories. **a**. Freight transport route categories derived from the combined road and vessel density map. National borders and land-sea borders are also shown. **b**. Some of the estimated freight transport routes to Tokyo for explanatory purposes.

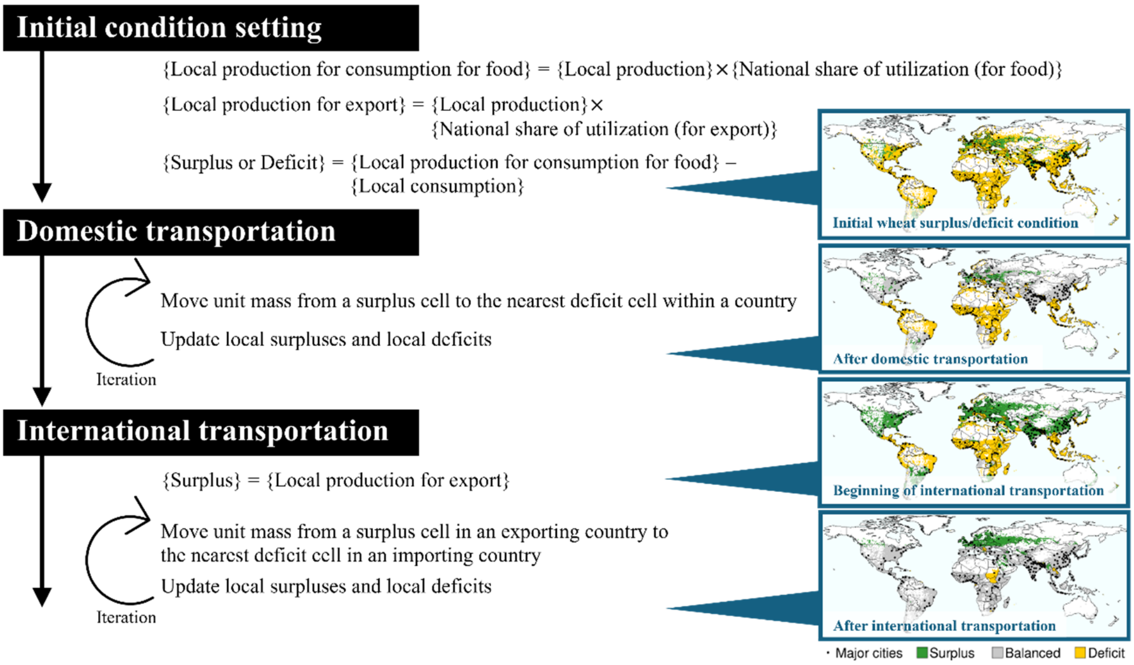

Supplementary Fig. 11. Schematic illustrating the procedure to estimate food-miles.